Available online at www.sciencedirect.com
ScienceDirect
Chemical Engineering and Processing 47 (2008) 1484–1491
Chemical Engineering and Processing Process Intensification
www.elsevier.com/locate/cep

Determination of the interfacial area of a continuous integrated mixer/separator (CINC) using a chemical reaction method

B. Schuur, W.J. Jansma, J.G.M. Winkelman, H.J. Heeres *

Department of Chemical Reaction Engineering, University of Groningen, Nijenborgh 4, 9747 AG Groningen, The Netherlands

Received 3 April 2007; received in revised form 15 May 2007; accepted 26 May 2007
Available online 3 August 2007

Abstract

The effect of the liquid flow rates (18–100 mL/min) and rotor frequency (30–60 Hz) on the interfacial area of a liquid–liquid system in a CINC-V02 continuous integrated mixer/separator have been studied using a chemical reaction method. Typical specific interfacial areas were in the range of 3.2×10^2 to 1.3×10^4 m^2 m^{-3} liquid volume, which is comparable with those for a continuously stirred tank reactor (CSTR). A pronounced maximum in the interfacial area with respect to the rotor frequency was found at about 45 Hz. The interfacial area increased considerably at higher aqueous phase flow rates whereas the organic phase flow rate had no significant effect. The experimental data were modelled using an empirical model. Good agreement between experiments and model was observed.

Keywords: Process intensification; CINC; Interfacial area; Chemical reaction method

1. Introduction

Process intensification is a powerful concept to replace large, energy intensive equipment or processes with smaller plants that combine multiple operations in single, highly integrated devices [1]. Examples are reactive distillation [2] and reactive extraction [2]. For the latter, the integration of reaction and separation is not only advantageous with respect to energy and investments costs but also to the efficiency and/or the selectivity of the extraction process [3–5].

A very attractive device to integrate chemical reaction and separation is the CINC integrated mixer/separator [6]. The CINC basically consists of a rotating hollow centrifuge in a static housing (Fig. 1). The liquid(s) enter the device in the annular zone between the static wall and the rotating centrifuge, where they are intensely mixed. Next, they are transferred into the centrifuge where separation occurs by the action of centrifugal forces [7]. The centrifugal forces can be as high as $900 \times g$, allowing excellent phase separation even when the densities of the phases differ only slightly. A cutaway view of the CINC is depicted in Fig. 1.

The CINC device was initially developed for oil spill clean up. Further applications were developed in the field of liquid–liquid separation and extraction (e.g. metal extractions) [2]. The equipment is available in different sizes and may be operated in a wide volumetric flow window (10^{-5} to 50 m^3/h). When required, a number of CINC's may be interconnected for multistage operation.

The CINC device is potentially very attractive for the integration of reaction and separation. To the best of our knowledge the device has not been applied for this application yet.

We have recently demonstrated the application of the CINC for the continuous biphasic enzyme catalyzed (*Rhizomucor miehei* lipase) esterification of oleic acid with *n*-butanol in a heptane/water mixture [7]. Oleic acid conversions of up to 70% were obtained when operating at full recycle of the aqueous, enzyme containing, stream and partial recycle of the organic stream.

We have also studied racemate separation in the CINC-V02 using reactive liquid–liquid extraction with chiral extractants. Racemate separation is of pivotal importance for the fine chemical and pharmaceutical industry. Very promising results were obtained for the enantioselective extraction of 3,5-dinitrobenzoyl-D,L-leucine (DNB-D,L-leu) using a cinchona alkaloid extractant. A non-optimized enantiomeric excess (ee) of 52% in the organic phase at 35% yield was obtained in once through operation [8].

* Corresponding author. Tel.: +31 50 363 4174; fax: +31 50 363 4479.
E-mail address: h.j.heeres@rug.nl (H.J. Heeres).

0255-2701/$ – see front matter © 2007 Elsevier B.V. All rights reserved.
doi:10.1016/j.cep.2007.05.028

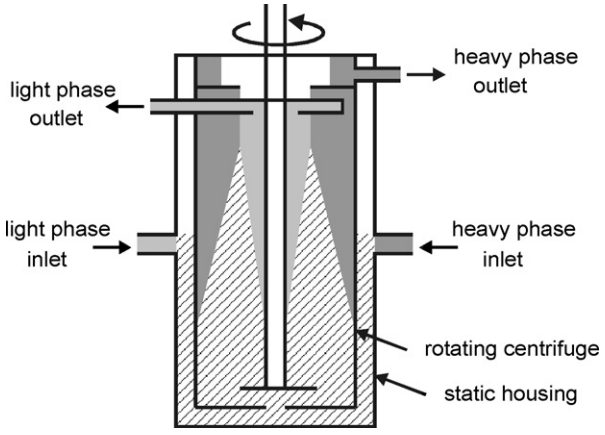

Fig. 1. Cutaway view of the CINC, hatched: dispersion, darker gray: heavy phase, lighter gray: light phase.

Optimization of these novel applications in the CINC as well as existing applications in the field of solvent separation require detailed scientific knowledge about the hydrodynamics in the devices like liquid flow patterns, liquid hold-ups in the various zones and the liquid–liquid interfacial area.

Here we report experimental results on the interfacial area in the CINC as a function of process conditions (flow rates and rotational speed of the centrifuge). The interfacial area can be determined both by direct measurements (imaging) [9] and indirect methods such as UV permeability measurements [10] and a liquid–liquid biphasic chemical reaction [11]. Since imaging and permeability measurements are not possible in the CINC because of its steel walls, in this study the reaction between *n*-butyl formate and sodium hydroxide [11] was used for determination of the total interfacial area. This reaction was selected as the kinetics as well as the relevant physical properties of the reactants (like diffusivity) are all known with good accuracy.

2. Experimental

2.1. Chemicals

NaOH pellets, 0.100 M HCl (Titrisol) and *n*-butanol were obtained from Merck, *n*-butyl formate was obtained from Aldrich, acetone (AR) from Labscan Ltd., *n*-octane from Janssen Chimica and N_2 (>99.99%) from Hoek Loos. Reverse osmosis water was applied to prepare the NaOH and HCl solutions.

2.2. Experimental set-up

All experiments were carried out under a nitrogen atmosphere in a CINC-V02 (a table top version with a maximum total throughput of 2 L min^{-1} (3.3×10^{-5} m^3 s^{-1}) and maximum rotational frequency of 100 Hz) made from Hastelloy and equipped with a heating/cooling jacket. The reaction temperature was kept under 300 K (typically 295–298 K) by cooling with water. Both liquids were transferred to the reactor using Verder VL1000 Control peristaltic tube pumps equipped with double pump heads ($1.6 \times 1.6 \times 8$R). All supply and receive vessels were made out of glass and kept under a nitrogen atmosphere.

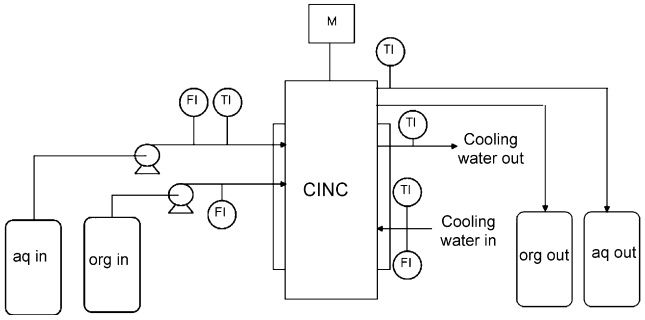

Fig. 2. Schematic representation of the experimental setup.

The aqueous in- and outlet streams and the cooling water in- and outlet streams were equipped with temperature sensors (CMA, Amsterdam) connected with a PC via a CoachLab II interface (CMA, Amsterdam). Aqueous and organic phase inlet flows, as well as the cooling water flow were measured with flow meters. A schematic representation of the setup is provided in Fig. 2.

2.3. Experimental procedure

The NaOH-solutions were made by dissolving NaOH pellets in RO-water. *n*-Butyl formate was used as received. Prior to the experiments, the supply and receive vessels were flushed with nitrogen gas (three times) and subsequently the solutions were bubbled with nitrogen at least 4 h to ensure the system was free of CO_2. The cooling water rate was set at 1.1 L min^{-1} and the temperature measurement was started. After 1 h a nitrogen atmosphere was applied to the CINC, and the pump of the aqueous solution and the centrifuge were started. When the reactor was filled with the aqueous solution and water appeared from the aqueous phase outlet, the organic phase pump was started. As soon as the organic phase reactor outlet started running, samples were collected every 2 min during 20 min. The flow rates were registered at regular time intervals. After 20 min, the measurements were stopped.

2.4. Analytical procedures

Organic phase samples were analyzed by GC-FID using an HP 5890 series II plus GC apparatus equipped with an HP-5 column (30 m length, 0.25 mm diameter and 0.25 μm film thickness) and an HP 7673 GC-SF injector. The GC measurements were carried out isothermally at a column temperature of 60 °C, injection and detection temperatures were 250 °C. Samples for analysis were made by mixing 0.08 g of the organic phase with 1.00 g of a 0.2 wt.% octane solution in acetone.

2.5. Model development

The operating variables of interest are the flow rates of both phases and the rate of rotation of the centrifuge. The significance of these variables on the variance of the total interfacial area was analysed statistically using Design Expert 7 software (Stat-Ease). The total interfacial area was modeled for this purpose

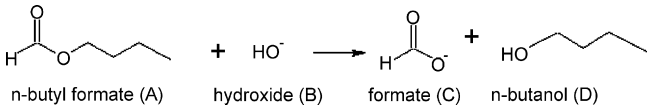

Fig. 3. Saponification of *n*-butyl formate using hydroxide.

using a standard expression as given in the following equation:

$$y = b_0 + \sum_{i=1}^{3} b_i x_i + \sum_{i=1}^{3}\sum_{j=i}^{3} b_{ij} x_i x_j \quad (1)$$

The operating variables N, F_{aq} and F_{org} are represented by the indices 1–3. The regression coefficients were obtained by statistical analyses of the data. Significance of factors was determined by their p value in the ANOVA analyses. A factor was considered significant if the p value was lower than 0.05, meaning that the probability of noise causing the correlation between a factor and the response is lower than 0.05. Insignificant factors were eliminated using backward elimination. The significant factors were used to fit a linear model to the data.

3. Theory

The selected reaction to determine the total interfacial area in the CINC device is represented in Fig. 3. The saponification of butyl formate is irreversible and first order in butyl formate and in the hydroxide-ion. The reaction takes place in the aqueous phase and butyl formate has to transfer from the butyl formate phase to the aqueous phase to react (Fig. 4).

The total interfacial area may be determined from the amount of A transferring from the organic phase to the aqueous phase. This quantity may be obtained from a mass balance of compound B in the aqueous phase. When assuming that the liquid phases are fully backmixed [12], the mass balance of compound B in the aqueous phase is given by:

$$V_R \varepsilon_{aq} \frac{dC_{B,aq}}{dt} = \phi_{v,aq,in} C_{B,aq,in} - \phi_{v,aq,out} C_{B,aq,out} + R_B \varepsilon_{aq} V_R \quad (2)$$

The reaction rate of B is correlated to the flux of A by the following relation:

$$R_B \varepsilon_{aq} V_R = -J_A A_{tot} \quad (3)$$

Combination of Eqs. (2) and (3) and when operating at steady-state conditions, Eq. (2) simplifies to

$$J_A A_{tot} = \phi_{v,aq,in} C_{B,aq,in} - \phi_{v,aq,out} C_{B,aq,out} \quad (4)$$

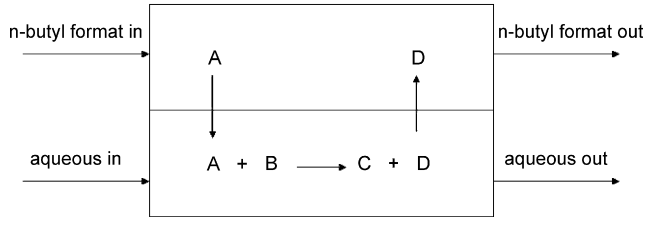

Fig. 4. Representation of the biphasic reaction applied in this study.

According to the film theory, the flux of A through the interface is given by [13]:

$$J_A = k_{L,aq} C^*_{A,aq} E_A \quad (5)$$

Here $C^*_{A,eq}$ is the interfacial concentration of A ($C^*_{A,aq} = m_A C_{A,org}$) and E_A is the enhancement factor for mass transfer. E_A is a function of the regime of mass transfer, for which information may be obtained using the Hatta number [13]. For irreversible reactions of a 1,1 stoichiometry, the Hatta number is given by

$$Ha = \frac{\sqrt{k_{1,1} C_{B,aq} D_A}}{k_{L,aq}} \quad (6)$$

In case Ha is smaller than 0.3, the reaction takes place in the slow regime and E_A is equal to 1. In the fast regime ($2 < Ha \ll E_{A\infty}$), Eq. (7) is valid:

$$E_A = Ha = \frac{\sqrt{k_{1,1} C_{B,aq} D_A}}{k_{L,aq}} \quad (7)$$

Here $E_{A\infty}$ is the instantaneous enhancement factor, which is defined as

$$E_{A\infty} = 1 + \frac{D_B C_B}{D_A m_A C^*_{A,org}} \quad (8)$$

In the instantaneous regime ($Ha > E_{A\infty}$), E_A equals $E_{A\infty}$.

In case the reaction takes place in the fast regime (Eq. (7)), the flux is not a function of the unknown mass transfer coefficient (see Eq. (5)). In this regime, the liquid–liquid interfacial area may be determined using Eq. (3), provided that the physico-chemical parameters such as the rate constant and the diffusivities are known.

When using this approach, the following considerations should be taken into account. Transport limitations in the organic phase should be avoided to simplify the equations. For this purpose, pure *n*-butyl formate (A) is applied. The interfacial concentration of A may thus be written as

$$C^*_{A,aq} = m_A C_{A,org} \quad (9)$$

Diffusion limitation of B in the aqueous phase should be avoided, which holds if the concentration of B is very large compared to the concentration A in the aqueous phase. In addition, when using a large excess of B, the reaction can be considered as a pseudo-first order reaction in A. This considerably simplifies the equations. Furthermore, the concentration of product should remain low to avoid dilution of the organic phase and the possible introduction of mass transfer resistance in the organic phase. For this purpose, the conversion of B was kept always below 0.15 [11]. Here, the conversion of B is defined as

$$X_B = \frac{C_{B,aq,in} - C_{B,aq,out}}{C_{B,aq,in}} = \frac{\phi_{v,aq}}{\phi_{v,org}} \frac{C_{D,org}}{C_{B,aq,in}} \quad (10)$$

When these requirements are met, the interfacial area follows from Eqs. (4)–(7) and (9):

$$A_{tot} = \frac{\phi_{v,aq,in} C_{B,aq,in} - \phi_{v,aq,out} C_{B,aq,out}}{m_A C_{A,org} \sqrt{k_{1,1} C_{B,aq,out} D_A}} \quad (11)$$

4. Physico-chemical parameters

The ionic strength of the aqueous phase is calculated using Eq. (12). Here, it is assumed that the system is completely free of CO_2:

$$I = \tfrac{1}{2}(C_{Na^+} z_{Na^+}^2 + C_{OH^-} z_{OH^-}^2 + C_{HCOO^-} z_{HCOO^-}^2) \quad (12)$$

$HCOO^-$ and OH^- are related by the reaction stoichiometry and therefore Eq. (12) simplifies to

$$I = \tfrac{1}{2}(C_{Na^+} z_{Na^+}^2 + C_{OH^-} z_{OH^-}^2)_{aq,in} \quad (13)$$

The viscosity of the aqueous NaOH solution is related to the viscosity of pure water by using the correlation of Onda et al. [14]:

$$\mu_{aq} = \mu_w(1 + 0.177I + 0.0527I^2) \quad (14)$$

The viscosity of water is calculated using [11]:

$$\log(\mu_w) = \frac{1.3271(293.15 - T) - 0.001053(T - 293.15)^2}{T - 168.15} - 3 \quad (15)$$

The diffusion coefficient of butyl formate ester in the aqueous phase is a function of temperature and the concentration of sodium hydroxide in the aqueous phase. The Wilke–Chang method [15] is used to estimate the diffusion coefficient of butyl formate in water (Eq. (16)). The diffusion coefficient of butyl formate in an aqueous solution of sodium hydroxide [14] is subsequently correlated to the diffusion coefficient in water using Eq. (17):

$$D_{A,w} = 2.67 \times 10^{-15} \frac{T}{\mu_w} \quad (16)$$

$$D_{A,aq} = \frac{D_{A,w}}{1 + 0.118413I + 0.0217124I^2} \quad (17)$$

The pseudo-first-order reaction rate constant is given by [11]:

$$k_{1,1} = 9.02 \times 10^7 \, e^{-((36.2 \times 10^6/RT) + 0.33I)} \quad (18)$$

The second term in the exponent of this equation accounts for the effect of the ionic strength of the aqueous phase on the reaction rate.

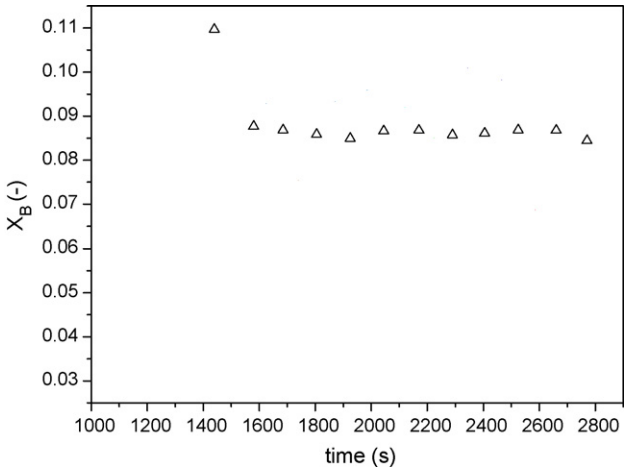

Fig. 5. Conversion of B in time.

From their experimental results, van Woezik et al. [11] obtained the value of the parameter group $m_A\sqrt{k_{11}D_A}$ as

$$m_A\sqrt{k_{11}D_A} = e^{(-2.05-(3350/T)-0.65I)} \quad (19)$$

From this, the partition coefficient, m_A, was calculated using the reaction rate constant and diffusivity given above.

5. Results and discussion

5.1. Determination of the total interfacial area in the reactor

The model reaction (Fig. 3) was carried out in the CINC using various flow rates and rotational speeds of the centrifuge (Table 1). The conversion profiles of OH^- (B) for a typical experiment are depicted in Fig. 5. The conversion of OH^- was calculated by determination of the concentration D in the organic phase using GC-FID (see Eq. (10)). A typical conversion profile is provided in Fig. 5. Only after the organic phase reactor outlet started running, the conversion measurements were started. The measurement that was taken before steady-state was achieved shows a higher conversion than in steady-state. This is due to the start-up procedure, in which the organic hold up has to build

Table 1
Overview of experimental conditions and results

Experiment	F_{org} (mL/min)	F_{aq} (mL/min)	N (Hz)	T (K)	$C_{B,in}$ (kmol m^{-3})	X_B	A (m^2)[a]
1	36	29	30	295	5.64	3.60×10^{-2}	0.11
2	35	29	30	295	5.64	1.75×10^{-2}	0.057
3	36	29	40	296	8.86	5.49×10^{-2}	1.51
4	33	28	40	296	8.81	5.53×10^{-2}	1.44
5	71	24	60	297	7.37	1.28×10^{-2}	0.12
6	72	18	60	298	7.65	4.66×10^{-2}	0.33
7	31	30	60	296	7.82	2.46×10^{-2}	0.38
8	34	30	60	296	7.82	1.83×10^{-2}	0.29
9	52	48	60	296	7.56	3.35×10^{-2}	0.68
10	41	48	60	298	7.10	4.67×10^{-2}	0.62
11	100	75	60	294	7.35	1.11×10^{-1}	2.41
12	45	49	60	300	8.49	9.65×10^{-3}	0.18

[a] The total interfacial area was calculated using Eq. (11).

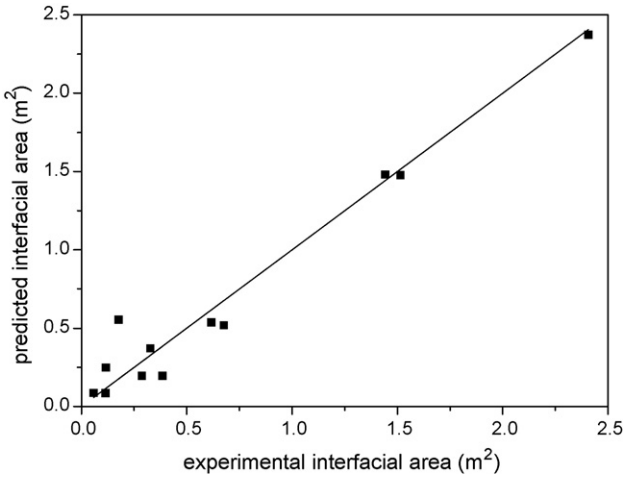

Fig. 6. Parity plot of the experimental and modeled interfacial area.

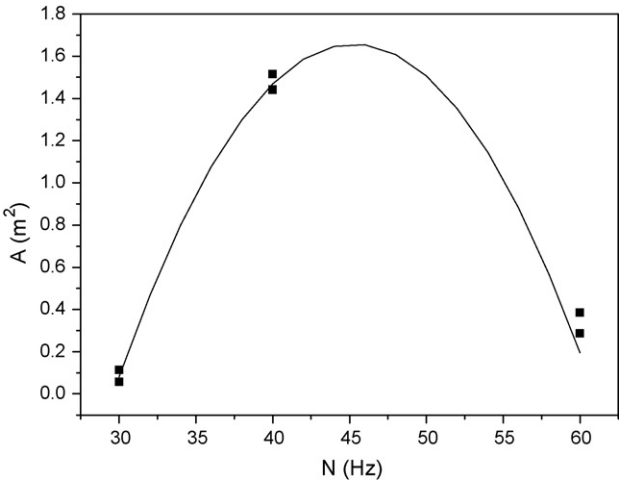

Fig. 7. The total interfacial area vs. the rate of rotation of the centrifuge at constant aqueous flow rate of 30 mL/min. Dots: experimental, line: Eq. (20).

up towards steady-state, causing the residence time being longer than the residence time in steady-state.

5.2. Quantification of the effect of process variables on interfacial area

To quantify the effect of the process variables on the interfacial area, the total interfacial area was modeled as described in Section 2.5. After elimination of the insignificant factors, the following model was fitted to the data:

$$A_{\text{mod}} = -11.14 + 0.612N - 0.0685F_{\text{aq}} - 6.76 \times 10^{-3}N^2 + 1.1 \times 10^{-3}F_{\text{aq}}^2 \quad (20)$$

Remarkably, factors including the variable F_{org} were insignificant, therefore this variable is not included in the model. A parity plot of the experimental and modeled data is provided in Fig. 6. Agreement is good ($R^2 = 0.9775$) implying that the total interfacial area is a strong function of the aqueous flow rate and the rate of rotation of the centrifuge.

5.3. Effect of the operating variables on the total interfacial area

In Fig. 7, the effect of the rotational speed of the centrifuge on the interfacial are is provided. The interfacial area shows a maximum at 40–50 Hz and is reduced considerably at lower and higher centrifugal speeds. To explain this pronounced effect, the mechanisms of both mixing and separation in the CINC devices should be considered. The observed total interfacial area is expected to be a function of the extent of mixing in the annular zone, affecting the average drop size, and the droplet settling velocity in the centrifuge zone, that will determine the volume of the dispersed phase in the centrifugal zone.

The extent of mixing in the annular zone is expected to be intensified at increasing rate of rotation. This will result in a lowering of the average drop size in the dispersion and an increase in the interfacial area. However, we clearly see that this explanation only holds for rotor speeds below 40–50 Hz. Apparently, another mechanism is operative, which leads to a reduction in the interfacial area when further increasing the rotor speed. This effect is likely related to the dynamics in the centrifugal zone. Three different zones are distinguishable in the centrifuge, one with the lighter of the two liquid phases, one with the heavier phase and a dispersed zone (Fig. 8). Besides the annular zone, the latter zone also contributes to the interfacial area in the CINC. The volumes of the various zones in the centrifuge are expected to be a function of the rate of rotation.

To gain insights in the volumes of the individual zones in the centrifuge, the settling velocity of individual drops will be considered. For centrifugal settlers such as in the CINC, the settling velocity is given by Eq. (21) [16]:

$$v_{\text{S,CINC}} = \frac{d_{\text{d}}^2(\rho_{\text{d}} - \rho_{\text{c}})\omega^2 r}{18\mu_{\text{c}}} \quad (21)$$

The settling velocity is thus proportional to the difference in density and the angular acceleration, and proportional to the squared drop diameter. Due to the proportionality of the settling velocity with the angular momentum, we can expect that the volume of the dispersed phase in the centrifuge will be reduced considerably at high rotational speeds. This reduction in the volume of the dispersed phase at increasing rotational speeds most likely accounts for the observed reduction in total interfacial area at higher rotor speeds. Apparently, in the range below 40–45 Hz, reduction of the average drop size at increasing rotational speeds leading to higher interfacial areas has more impact than a reduction of the volume of the dispersed zone in the centrifuge.

The effect of the aqueous flow rate on the interfacial area is best visualized by plotting the total interfacial area at constant rate of rotation of the centrifuge versus the flow rate of the aqueous phase. A typical example is given in Fig. 9.

The total interfacial area increases strongly at higher aqueous flow rates. The maximum experimentally observed total interfacial area was 2.41 m^2 at an aqueous flow rate of 75 mL min^{-1}. This effect is best explained by considering the amount of dispersed phase in the centrifugal zone (Fig. 8). At higher liquid

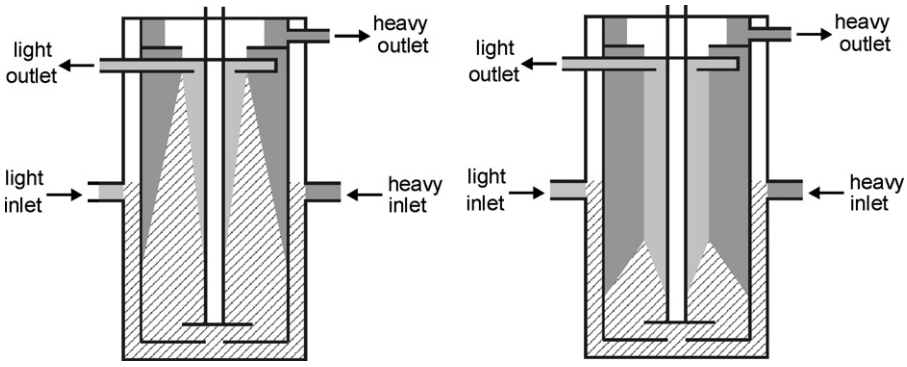

Fig. 8. Cross-sectional view on the CINC for a low (left) and a fast rotational speed (right) of the centrifuge. Hatched: dispersion, darker gray: heavy phase, lighter gray: light phase.

velocities in the centrifuge, an increase in the volume of the dispersed zone and thus the interfacial is expected. Further enlargement of the interfacial area by further increasing the aqueous liquid flow rate is limited by the separation capacity. At too high flow rates, quantitative separation of the two immiscible liquids is not possible.

It was experimentally observed that the organic flow rate has no significant effect on the total interfacial area. This observation suggests that the organic phase is the continuous phase and the water phase the dispersed phase. Further experiments with a modified CINC-V02, including electrodes to measure the conductivity, are in progress to confirm this statement.

5.4. Determination of the specific interfacial area

For comparability, the interfacial area of a liquid–liquid system is commonly expressed in terms of specific interfacial area ($m^2\,m^{-3}$ reactor volume or $m^2\,m^{-3}$ dispersion). For the CINC, the volume of the dispersion is not known quantitatively. However, information on the liquid hold-up as well as the geometrical volume of the reactor is available. Therefore, the specific interfacial area is expressed per m^3 total liquid volume in the reactor. The total liquid holdup has been determined experimentally at $1.8 \times 10^{-4}\,m^3$, essentially independent of the liquid throughputs. On the basis of these data and the experimentally determined total interfacial area (A), the specific interfacial areas as a function of process conditions are determined (Table 2).

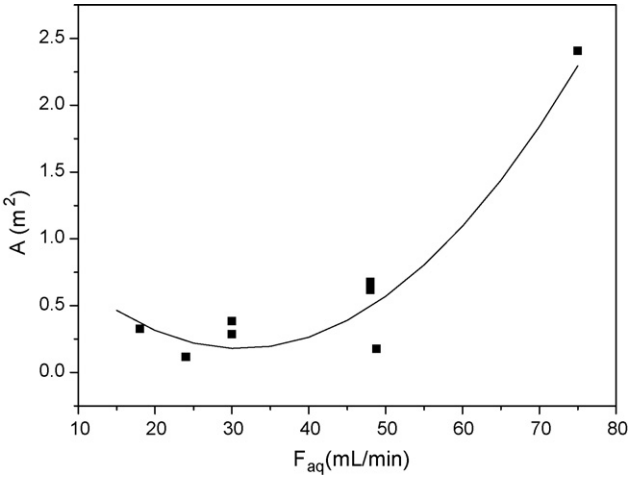

Fig. 9. Total interfacial area vs. the aqueous flow rate at constant rate of rotation of 60 Hz. Dots: experimental, line: Eq. (20).

The specific interfacial area in the CINC ranged from 3.2×10^2 to $1.3 \times 10^4\,m^2\,m^{-3}$ liquid volume, which is comparable to those reported for CSTR's [17,11] and much larger than, for example a spray or packed column [18] or a type of impinging jet reactor [19,20].

5.5. Validity of reaction regime

The calculation of the total interfacial area is only justified in case the reaction takes place in the fast regime, thus $2 < Ha < E_{A\infty}$. Calculation of the Hatta number is though, not possible, because the mass transfer coefficient $k_{L,A,aq}$ is not known for the CINC. Therefore the guidelines presented by Trambouze et al. [21] for mass transfer coefficients in liquid–liquid systems were used to estimate the range for the values of the mass transfer coefficients of A in the CINC.

For diffusion coefficients ranging from $D_{min} = 1 \times 10^{-9}$ to $D_{max} = 5 \times 10^{-9}\,m^2/s$, the liquid mass transfer coefficient typically has values between $k_{L,min} = 5 \times 10^{-5}$ to $k_{L,max} = 5 \times 10^{-4}$ m/s. However, the diffusivity of butyl formate ester in concentrated sodium hydroxide solutions is much lower and in the order of $10^{-11}\,m^2/s$, and therefore typical mass trans-

Table 2
Experimentally determined specific interfacial areas as a function of process conditions

Experiment	A (m^2)	a_L ($m^2\,m^{-3}$ total liquid volume)
1	0.11	6.3×10^2
2	0.057	3.2×10^2
3	1.51	8.4×10^3
4	1.44	8.0×10^3
5	0.12	6.4×10^2
6	0.33	1.8×10^3
7	0.38	2.1×10^3
8	0.29	1.6×10^3
9	0.68	3.8×10^3
10	0.62	3.4×10^3
11	2.41	1.3×10^4
12	0.18	9.9×10^2

Table 3
The minimum and maximum Hatta number and $E_{A\infty}$ values for each experiment

Experiment	Ha_{min}	Ha_{max}	$E_{A\infty}$
1	6.5	323	381
2	6.5	325	402
3	7.6	382	2016
4	7.6	380	1971
5	7.5	373	1055
6	7.6	381	1063
7	7.4	371	1315
8	7.5	375	1338
9	7.3	366	1108
10	7.4	369	827
11	6.9	343	761
12	7.9	395	1127

fer coefficients are also expected to be much less than 5×10^{-5} to 5×10^{-4} m/s. An estimation of the range of $k_{L,A,aq}$ values is obtained using Eq. (22) and a D_A of 10^{-11}:

$$\frac{D_A}{D_{max}} \cdot k_{L,min} < k_{L,A,aq} < \frac{D_A}{D_{min}} \cdot k_{L,max} \quad (22)$$

with the range of $k_{L,A,aq}$ values available, the Hatta numbers may be calculated using Eq. (6). For all experiments, the minimum and maximum value for Hatta and $E_{A\infty}$ are listed in Table 3. It may be concluded that all reactions were performed in the fast regime ($2 < Ha < E_{A\infty}$) and that the relation $E_A = Ha$ was valid.

6. Conclusions

The specific interfacial area in the CINC-V02 integrated mixer/separator was determined as a function of process variables using the chemical reaction method. The liquid flow rates were varied from 18 to 100 mL min^{-1} each, the rotor frequency from 30 to 60 Hz. The experimentally determined specific interfacial area was found to vary from 3.2×10^2 to 1.3×10^4 m^2 m^{-3} liquid volume, which is comparable with the specific interfacial area in a CSTR. The effects of the process conditions on the interfacial area were quantified using statistical methods and agreement between model and experiments was very satisfactorily.

The rate of rotation of the centrifuge and the flow rate of the aqueous phase both have significant effects on the specific interfacial area. However, the specific interfacial area was independent of the organic flow rate, suggesting that the organic phase is the continuous phase and the aqueous phase is the dispersed phase in the CINC device. The interfacial area showed a clear maximum (2.41 m^2) at intermediate rate of rotation of the centrifuge (40–50 Hz), which was ascribed to several opposing effects in the centrifuge and annular zone.

The results described here will be valuable input for subsequent modeling and optimization studies for classical CINC applications like liquid–liquid separation as well as new and exiting applications in the field of combined reaction and separation.

Acknowledgement

The research was financially supported by: the Dutch Foundation for Scientific Research (NWO) through the Separation Technology program in cooperation with DSM and Organon.

Appendix A. Nomenclature

a	specific interfacial area (m^2 m^{-3})
A_{tot}	total interfacial area
C	concentration (kmol m^{-3})
d	drop diameter (m)
D	diffusion coefficient (m^2 s^{-1})
E_A	enhancement factor
$E_{A\infty}$	asymptotic enhancement factor
E_{act}	energy of activation (J kmol^{-1})
F	volumetric flow rate (mL min^{-1})
g	gravitational constant (m s^{-2})
Ha	Hatta number
I	ionic strength (kmol m^{-3})
J	molar flux (kmol m^{-2} s^{-1})
k	mass transfer coefficient (m s^{-1})
$k_{1,1}$	rate of the reaction (m^3 kmol^{-1} s^{-1})
k_I	ionic strength reaction rate constant (m^3 kmol^{-1})
k_∞	preexponential constant (m^3 kmol^{-1} s^{-1})
m	partition coefficient
N	rate of rotation (Hz)
R	rate of production (kmol s^{-1})
R	gas constant = 8315 J kmol^{-1} K^{-1}
T	temperature (K)
v_S	settling velocity (m s^{-1})
V	volume (m^3)
X	conversion
z	charge of ion

Greek letters

ε	volume fraction of total reactor volume (m^3 m^{-3})
μ	viscosity (N s m^{-2})
ρ	density (kg m^{-3})
ϕ_v	volumetric flow rate (m^3 s^{-1})
ω	angular velocity (rad s^{-1})

Superscripts

*	interfacial

Subscripts

aq	aqueous phase
A	component A, i.e. *n*-butyl formate
B	component B, i.e. ionic hydroxide
c	continuous phase
d	dispersed phase
G	geometrical
in	inlet
L	liquid
min	minimum value
max	maximum value

org	organic phase
out	outlet
R	reactor
w	water

References

[1] A. Stanckiewicz, J.A. Moulijn, Re-engineering the Chemical Processing Plant; Process Intensification, Marcel Dekker, Inc., New York, 2004.

[2] E.Y. Kenig, A. Gorak, H.J. Bart, in: A. Stanckiewicz, J.A. Moulijn (Eds.), Re-Engingeering the Chemical Processing Plant; Process Intensification, Marcel Dekker, Inc., New York, 2004, pp. 309–378.

[3] J.C. Godfrey, M.J. Slater, Liquid–Liquid Extraction Equipment, John Wiley & Sons, New York, 1994.

[4] C. Hanson, Recent Advances in Liquid–Liquid Extraction, Pergamon Press Ltd., 1971.

[5] J.D. Thornton, Science and Practice of Liquid–Liquid Extraction, Clarendon, Oxford, 1992.

[6] D.H. Meikrantz, L.L. Macaluso, H.W. Sams, C.H. Schardin, A.G. Federici, US Patent 5,762,800 (June 9, 1998).

[7] J.G. de Vries, G.N. Kraai, B. Schuur, F. van Zwol, H.J. Heeres, Continuous chemical production in an integrated reactor/separator device, in preparation.

[8] B. Schuur, J.G. de Vries, H.J. Heeres, Continuous enantioselective extraction of 3,5-dinitrobenzoyl-D,L-leucine in an integrated mixer/separator, in preparation.

[9] L.L. Tavlarides, M. Stamatoudis, in: T.B. Drew, G.R. Cokelet, J.W. Hoopes, T. Vermeulen (Eds.), Advances in Chemical Engineering, vol. 11, Academic Press, New York, 1981, pp. 199–273.

[10] H. Watarai, L. Cunningham, H. Freiser, Automated-system for solvent-extraction kinetic-studies, Anal. Chem. 54 (1982) 2390–2392.

[11] B.A.A. van Woezik, K.R. Westerterp, Measurement of interfacial areas with the chemical method for a system with alternating dispersed phases, Chem. Eng. Proc. 39 (2000) 299–314.

[12] B. Schuur, G.N. Kraai, J.G.M. Winkelman, H.J. Heeres, Hydrodynamics in a CINC device, in preparation.

[13] K.R. Westerterp, W.P.M. van Swaaij, A.A.C.M. Beenackers, Chemical Reactor Design and Operation, Wiley, Chichester, 1987.

[14] K. Onda, H. Takenchi, M. Fujine, Y. Takanashi, Study of mass transfer between phases by a diaphragm cell—alkaline hydrolysis of esters in aqueous NAOH solution, J. Chem. Eng. Jpn. 8 (1975) 30–34.

[15] C.R. Wilke, P. Chang, Correlation of diffusion coefficients in dilute solutions, AIChE J. 1 (1955) 264–270.

[16] R.H. Perry, D.W. Green, J.O. Maloney, Perry's Chemical Engineers' Handbook, 7th, McGraw-Hill, New York, 1997.

[17] M.D. Santiago, P. Trambouz, Perfectly agitated reactors with 2 liquid phases—measurement of interfacial area by chemical method, Chem. Eng. Sci. 26 (1971) 29–38.

[18] S.A. Puranik, M.M. Sharma, Effective interfacial area in packed liquid extraction columns, Chem. Eng. Sci. 25 (1970) 257.

[19] A.M. Dehkordi, Liquid–liquid extraction with chemical reaction in a novel impinging-jets reactor, AIChE J. 48 (2002) 2230–2239.

[20] A.M. Dehkordi, Liquid–liquid extraction with an interphase chemical reaction in an air-driven two-impinging-streams reactor: effective interfacial area and overall mass-transfer coefficient, Ind. Eng. Chem. Res. 41 (2002) 4085–4093.

[21] P. Trambouze, H. van Landeghem, J.P. Wauquier, Chemical Reactors, Editions Technip, Paris, 1988.